Ag NPs induced near-infrared emission enhancement of Er^{3+}/Tm^{3+} codoped tellurite glass*

XIA Li-zhang (夏礼章), **ZHANG Yu** (张雨), **SHEN Xin-jie** (沈欣杰), **HUANG Bo** (黄波), **and ZHOU Ya-xun** (周亚训)**

College of Information Science and Engineering, Ningbo University, Ningbo 315211, China

(Received 18 January 2020; Revised 11 March 2020)

Ag nanoparticles (NPs) were introduced into Er^{3+}/Tm^{3+} codoped tellurite glasses prepared using melt-quenching and heat-treated techniques. The glass samples were characterized by the differential scanning calorimeter (DSC), X-ray diffraction (XRD), transmission electron microscopy (TEM) and photoluminescence to reveal the Ag NPs induced broadband near-infrared band emission enhancement of Er^{3+}/Tm^{3+} ions. The studied glasses possessed good thermal stability with ΔT larger than 137 ℃. For glass sample heat-treated at 360 ℃ for 6 h, the nucleated Ag NPs in near-spherical shape with an average diameter about 6.5 nm dispersed in the glass matrix. Under the excitation of 808 nm laser diode (LD), the broadband near-infrared fluorescence emission extending from 1 350 nm to 1 620 nm, owing to the combined contributions from the $^3H_4 \rightarrow {}^3F_4$ transition of Tm^{3+} at 1.47 μm band and the $^4I_{13/2} \rightarrow {}^4I_{15/2}$ transition of Er^{3+} at 1.53 μm band, improved significantly with the introduction of Ag NPs, which is mainly attributed to the increased local electric field. The present results indicate that Er^{3+}/Tm^{3+}/Ag NPs codoped tellurite glass with good thermal stability is a promising glass material for broadband fiber amplifiers of WDM transmission systems.

Document code: A **Article ID:** 1673-1905(2021)02-0080-5

DOI: https://doi.org/10.1007/s11801-021-0011-z

With the rapid development of optical communication and new occurred data-transmitting services in the wavelength-division-multiplexing (WDM) systems in recent years, the explosive increasing information traffic to be transmitted makes them urgent to improve the transmission capability[1-3]. As a key device to amplify the decay optical carrier signals, therefore, developing the broadband optical amplifiers is very necessary. Owing to the radiative transition of Tm^{3+}:$^3H_4 \rightarrow {}^3F_4$ centered at 1.47 μm band and that of Er^{3+}:$^4I_{13/2} \rightarrow {}^4I_{15/2}$ centered at 1.53 μm band, Er^{3+}/Tm^{3+} codoped glass materials pumped at 808 nm present the advantage of continuous optical spectrum covering the whole S+C bands (1 460—1 565 nm) and also extending to the short E-band (1 360—1 460 nm) and long L-band (1 565—1 625 nm), respectively[3-5], which provides a potentiality of broader optical communication band than the current conventional Er^{3+} doped fiber amplifier (EDFA). For example, Li et al[4] have reported an ultra-broadband fluorescence emission extending from 1 300 nm to 1 650 nm with a full width at half maximum (*FWHM*) of ~160 nm in Er^{3+}/Tm^{3+} codoped bismuthate glass. Zhu et al[5] have reported an ultra-broadband fluorescence emission from 1 350 nm to 1 650 nm with the *FWHM* around 148 nm in Er^{3+}/Tm^{3+} codoped tellurite glass.

Even though an ultra-broadband near-infrared fluorescence emission can be achieved in Er^{3+}/Tm^{3+} codoped glass systems, the fluorescence intensity of this broad band is relatively weak in comparison with the other emission bands (such as 1.85 μm band for Tm^{3+}) under the same pumping scheme. Thus, to improve the fluorescence emission intensity, coupling doped rare-earth ions with metallic nanoparticles (such as Ag NPs) is now developed due to the local surface plasmon resonance (LSPR) effect, which is classically characterized by the collective oscillation of conduction free electrons with respect to the positive core of NPs in the presence of light incidence[6,7]. When the frequency of incident light is resonant with the oscillation frequency of conduction free electrons, a significant enhancement of local electric field will occur in the vicinity of NPs and in turn improve the transition rates of doped rare-earth ions[8]. Tellurite glass appears as a good candidate to realize broadband emission in the near-infrared region owing to its excellent properties[9], such as wide transmission window, high rare-earth solubility, low phonon energy and high refractive index. The high refractive index can improve the stimulated absorption and emission cross-sections, and the low phonon energy can improve the radiative

* This work has been supported by the National Natural Science Foundation of China (No.61875095), the Natural Science Foundation of Ningbo City (No.2016A610061), and the K. C. Wong Magna Fund in Ningbo University.

** E-mail: zhouyaxun@nbu.edu.cn

quantum efficiency through suppressing the non-radiative relaxation processes of doped rare-earth ions.

In this work, Ag NPs were introduced into Er^{3+}/Tm^{3+} codoped tellurite glasses with conventional composition TeO_2-ZnO-Na_2O to improve the broadband fluorescence emission intensity in the near-infrared region for optical communication, and the effects of Ag NPs content on the thermal stability and near-infrared band emission properties of Er^{3+}/Tm^{3+} codoped tellurite glasses pumped by 808 nm LD were investigated. To the best of our knowledge, the improved studies of Ag NPs on the emission intensity of broadband near-infrared fluorescence from Er^{3+}/Tm^{3+} ions have rarely been reported.

Er^{3+}/Tm^{3+}/Ag NPs codoped tellurite glasses with molar compositions of 75TeO_2-15ZnO-(9-*x*)Na_2O-0.2Er_2O_3-0.8Tm_2O_3-*x*$AgNO_3$ (*x*=0, 0.25, 0.5 and 1 %) were synthesized using the melt-quenching and subsequent heat-treating technique. Batch of 10.0 g powder was weighed and ground thoroughly in an agate mortar to obtain homogeneous mixture. The well-mixed powder was placed in a platinum crucible and melted in an electric furnace at 900 ℃ for 1 h. Then, the melt was rapidly quenched by pouring it in a preheated brass mold. After, the glass sample was immediately transferred to a muffle furnace and annealed at 330 ℃ for 2 h to release the internal mechanical stress and then slowly cooled down to the ambient temperature. To thermally reduce Ag^+ ions to Ag^0 atoms and then nucleate and grow into the metallic Ag NPs, all the prepared glass samples were heat-treated at 360 ℃ for 6 h in the muffle furnace again.

The obtained samples were named as ET-A0, ET-A1, ET-A2 and ET-A3 according to the $AgNO_3$ amount respectively for clarity, and were then cut, polished and measured at room temperature. The thermal stability was measured using a differential scanning calorimeter (DSC) of TA Instrument Q2000 at a heating rate of 10 K/min. Powder X-ray diffraction (XRD) pattern was measured by a power diffractometer of Bruker D2 with Cu Ka radiation (40 kV×25 mA). The image of nucleated Ag NPs in glass matrix was captured by a transmission electron microscopy (TEM 2100, JEOL) with an acceleration voltage of 200 kV. Fluorescence emission spectrum was collected by a TRIAX 550 spectrophotometer upon excitation of 808 nm LD and UV/Vis/NIR absorption spectrum was recorded with a Perkin-Elmer-Lamda 950 spectrophotometer.

Thermal stability is an important indicator for laser glasses, especially for high doped laser glasses as they are easier to crystallization during the reheating process when drawing the fiber. The thermal stability of glass is usually characterized by the difference (ΔT=T_x−T_g) between the glass crystallization onset temperature (T_x) and transition temperature (T_g)[10]. A large ΔT indicates a strong suppression of crystallizing action, which means a wide range of working temperature can be allowed. Fig.1 displays the DSC curves of ET-A0 and ET-A2 glass samples as a representative in the range of 250—550 ℃, and the obtained three temperature parameters for all glass samples were listed in Tab.1. It was seen from the Table that both the T_x and T_g decreased slightly with the introduction of $AgNO_3$. The decreased T_g indicated the reduce of glass viscosity with the nucleation of Ag NPs in the glass network, which could be attributed to the structure compactness decline due to the presence of Ag NPs in the free space regions, while the decrease of T_x could be attributed to the formation of heterogeneous nucleation sites by Ag NPs for the major crystalline phases[11]. Nevertheless, the values of ΔT for all glass samples were still larger than 137 ℃. Generally, larger than 100 ℃ for ΔT can meet the requirement of conventional fiber drawing. Therefore, the studied Er^{3+}/Tm^{3+}/Ag NPs codoped tellurite glasses possessed good thermal stability and were appropriate for fiber drawing.

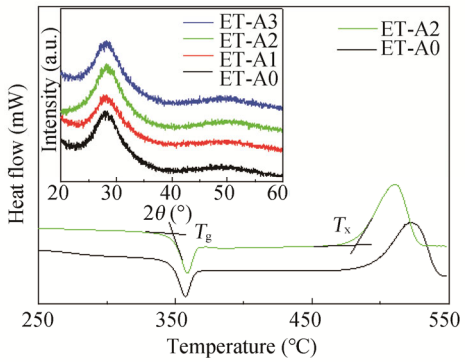

Fig.1 DSC curves of ET-A0 and ET-A2 glass samples, where inset is XRD patterns of ET-A*x* (*x*=0, 1, 2 and 3) glass samples

Tab.1 The *FWHM*, glass transition temperature (T_g), crystallization onset temperature (T_x) and the difference (ΔT) between them for prepared ET-A*x* (*x*=0,1,2 and 3) glass samples

Sample	*FWHM* (nm)	T_g (±0.5 ℃)	T_x (±0.5 ℃)	ΔT=T_x−T_g (±0.5 ℃)
ET-A0	90.2	348.9	495.7	146.8
ET-A1	89.5	347.8	491.2	143.4
ET-A2	89.8	347.5	485.1	137.6
ET-A3	91.3	345.3	482.6	137.3

The XRD patterns of glass samples are displayed in the inset of Fig.1. It was seen that all the XRD patterns exhibited the same feature: a broad hump in the range of 25°—35° with the absence of discrete diffraction peak, indicating the absence of structural periodicity. In other words, the structural nature of the studied glasses was amorphous state[12].

Fig.2(a) and (b) display the TEM image with resolution of 50 nm and the selected area electron diffraction (SAED) pattern of ET-A2 glass sample, respectively.

Near-spherical shape Ag NPs, which dispersed in the glass matrix, were revealed by the black particles with different sizes in the TEM image, and the bright spots in the SAED pattern also indicated the presence of Ag NPs, in which the spots in first, second and third rings corresponded to the (111), (200) and (220) plane reflections of silver NPs, respectively[13]. Fig.2(c) displays the size histogram of Ag NPs, which exhibited the Gaussian distribution behavior and an average diameter about 6.5 nm of Ag NPs was determined.

The Ag NPs in the glass matrix was originated from the thermo-chemical reduction reactions. The Ag^0 atoms first occurred during the glass melting process through the following reduction reactions[8]:

$$Ag^+ + e^- \rightarrow Ag^0, \quad Ag^+ + Ag^+ \rightarrow Ag^{2+} + Ag^0 . \tag{1}$$

In the tellurite glass, the thermo-chemical reduction from Ag^+ ions to Ag^0 atoms can be promoted by Te^{4+} ions as[14]

$$Te^{4+} + 2Ag^+ \rightarrow Te^{6+} + 2Ag^0. \tag{2}$$

Next, different sizes of metallic Ag NPs occurred through the nucleation of Ag^0 atoms and then growth via the mechanisms of Ostwald ripening and NPs migration followed by coalescence during the subsequent heat-treated process[15].

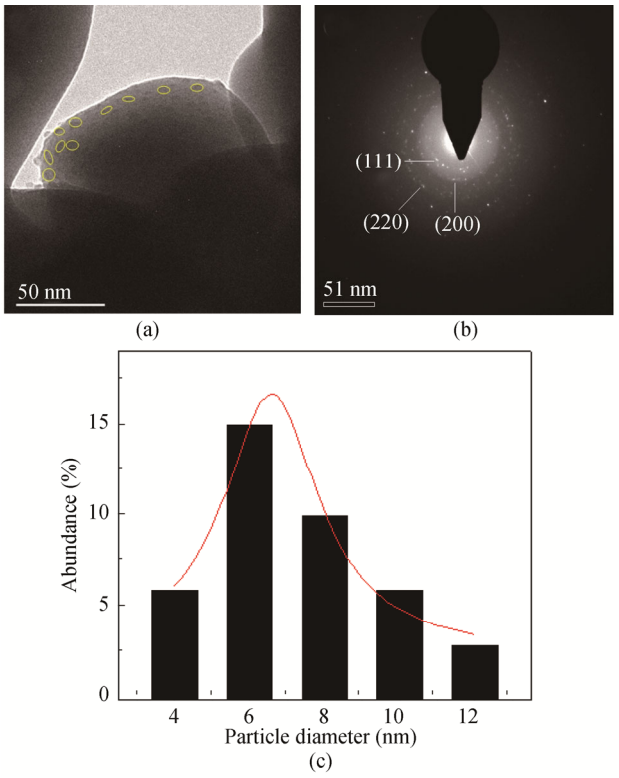

Fig.2 (a) TEM image with resolution of 50 nm; (b) SAED pattern of Ag NPs; (c) Histogram of size distribution of Ag NPs for the ET-A2 glass sample

The UV/Vis/NIR absorption spectrum of Er^{3+}/Tm^{3+}/Ag NPs codoped ET-A2 glass sample is displayed in Fig.3. The spectrum was labeled by the Er^{3+} and Tm^{3+} absorption bands, in which the bands centered at 1 532 nm, 980 nm, 793 nm, 652 nm, 545 nm, 523 nm, 486 nm and 449 nm were attributed to the absorption transitions from the ground state $^4I_{15/2}$ of Er^{3+} to the excited levels of $^4I_{13/2}$, $^4I_{11/2}$, $^4I_{9/2}$, $^4F_{9/2}$, $^4S_{3/2}$, $^2H_{11/2}$, $^4F_{7/2}$ and $^4F_{5/2}$, and the bands located at 1 703 nm, 1 213 nm, 793 nm, 686 nm and 466 nm were assigned to the absorption transitions from the ground state $^3H_6$ of Tm^{3+} to the excited levels of $^3F_4$, $^3H_5$, $^3H_4$, $^3F_{2,3}$ and $^1G_4$, respectively[4,5]. The strong absorption band at around 800 nm from both the Tm^{3+}:$^3H_6 \rightarrow ^3H_4$ and Er^{3+}:$^4I_{15/2} \rightarrow ^4I_{9/2}$ transitions indicated that the Er^{3+}/Tm^{3+} codoped tellurite glass can be pumped efficiently by 808 nm LD. However, the absorption band associated with the LSPR of Ag NPs could not be observed, which was attributed to the small amount of Ag NPs in the glass host as well as the intense absorption in the visible band of Er^{3+}/Tm^{3+} ions, and the other reason was the fact that the LSPR band itself was inherently weak in the tellurite glass systems[16].

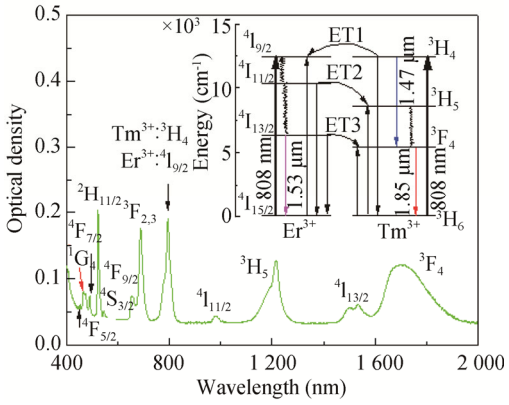

Fig.3 Absorption spectrum of Er^{3+}/Tm^{3+} codoped ET-A2 glass sample, where inset is the energy level diagram of Er^{3+} and Tm^{3+} ions and relevant transitions under the excitation of 808 nm LD

The fluorescence emission spectra of Er^{3+}/Tm^{3+}/Ag NPs codoped ET-Ax (x=0, 1, 2 and 3) glass samples in the wavelength range of 1 250—1 650 nm under the excitation of 808nm LD is displayed in Fig.4. An ultra-broadband near-infrared emission extending from 1 350 nm to 1 620 nm with the *FWHM* of ~90 nm, as listed in Tab.1, was observed owing to the $^3H_4 \rightarrow ^3F_4$ transition of Tm^{3+} at 1.47 μm band overlapping with the 1.53 μm emission band associated with the $^4I_{13/2} \rightarrow ^4I_{15/2}$ transition of Er^{3+}[5,17], while the 1.85 μm emission band corresponding to the Tm^{3+}:$^3F_4 \rightarrow ^3H_6$ transition was partly displayed in the present measured spectrum range. The observed near-infrared emission covered the E, S, C and L telecommunication bands depicted explicitly in the inset of Fig.4, which provided potential application prospects for ultra-broadband fiber amplifiers applied for WDM transmission systems.

It was shown that the ultra-broadband emission intensity enhanced significantly with the introduction of Ag NPs into Er^{3+}/Tm^{3+} codoped tellurite glasses. The enhancement of ultra-broadband fluorescence was mainly

attributed to the increased local electric field (LEF) induced by metallic Ag NPs[16,18]. It has been known that there exists the interaction of incident pump light and/or fluorescence with metallic NPs, which results in the oscillation of conduction free electrons of metallic NPs. Such oscillations induce a confined LEF around NPs due to the relative permittivity difference between the metallic silver and glass matrix, which leads to the increase of LEF due to the light focus and the metallic screening effect[18,19]. The enhanced LEF improved the excitation and radiation transition rates of doped rare-earth ions in the vicinity of Ag NPs, and therefore the emission intensity increased. It is worth noting that the energy transfers (ET) between Er^{3+} and Tm^{3+} ions were responsible for the observed ultra-broadband near-infrared emission, which was depicted explicitly in the inset of Fig.3. The dominant ET processes were described as follows:

$$\text{ET1: } Tm^{3+}:{}^3H_4+Er^{3+}:{}^4I_{15/2}\rightarrow Tm^{3+}:{}^3H_6+Er^{3+}:{}^4I_{9/2}\ , \quad (3)$$

$$\text{ET2: } Er^{3+}:{}^4I_{11/2}+Tm^{3+}:{}^3H_6\rightarrow Er^{3+}:{}^4I_{15/2}+Tm^{3+}:{}^3H_5\ , \quad (4)$$

$$\text{ET3: } Er^{3+}:{}^4I_{13/2}+Tm^{3+}:{}^3H_6\rightarrow Er^{3+}:{}^4I_{15/2}+Tm^{3+}:{}^3F_4. \quad (5)$$

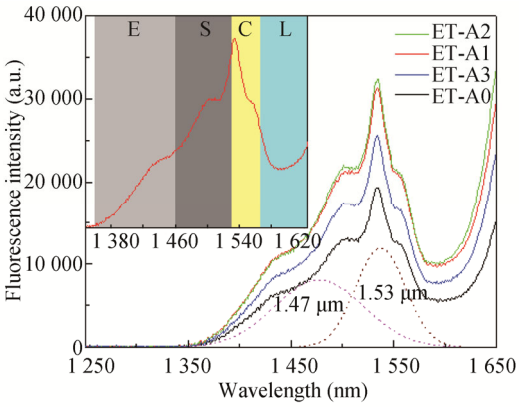

Fig.4 Near-infrared emission spectra of Er^{3+}/Tm^{3+} ions in ET-A*x* (*x*=0, 1, 2 and 3) glass samples, where inset highlights the detailed emission spectrum of ET-A1 glass sample in wavelength range of 1 350—1 620 nm

Under the excitation of 808 nm LD, Tm^{3+} ions at the ground state $^3H_6$ were pumped to the excited level $^3H_4$ by ground state absorption (GSA) process. Due to the energy matching, a part of Tm^{3+} at level $^3H_4$ brought about an effective energy transfer ET1 to the adjacent ground state Er^{3+} and excited the latter to the excited level $^4I_{9/2}$ as well as the GSA process of Er^{3+} themselves, while another part of Tm^{3+} at level $^3H_4$ radiated directly to the level $^3F_4$ generating the 1.47 μm band fluorescence. The Er^{3+} at level $^4I_{9/2}$ would rapidly return to the low-level $^4I_{11/2}$ through the multi-phonon relaxation (MPR) process, and a part of them transfered their energy to the adjacent ground state Tm^{3+} and excited the latter to the excited level $^3H_5$ through the energy transfer ET2, while the another part further relaxed to the low-level $^4I_{13/2}$ non-radiatively. Some of Er^{3+} ions at level $^4I_{13/2}$ radiated to the ground state $^4I_{15/2}$ emitting the 1.53 μm band fluorescence and the others transfered their energy to the level $^3F_4$ of Tm^{3+} through the energy transfer ET3. Finally, the 1.85 μm band fluorescence occurred when the Tm^{3+} at level $^3F_4$ radiated to the ground state $^3H_6$. In the current Er^{3+}/Tm^{3+} codoped tellurite glasses, however, the flatness of the obtained 1 350—1 620 nm ultra-broadband near-infrared emission spectrum was not ideal, which was important for WDM transmission system. Therefore, the concentration optimization between Er^{3+} and Tm^{3+} ions was necessary, which will be further studied in the later.

In summary, Er^{3+}/Tm^{3+} codoped tellurite glasses with various amounts of Ag NPs were prepared using the melt-quenching and subsequent heat-treated technique. Under the excitation of 808 nm LD, an appropriate amount of Ag NPs introduction can significantly improve the fluorescence intensity of near-infrared band emission from 1 350 nm to 1 620 nm, which is mainly attributed to the increased local field effect induced by Ag NPs. Therefore, the Er^{3+}/Tm^{3+}/Ag NPs codoped tellurite glasses have the promising prospects for broadband fiber amplifiers applied for WDM transmission systems.

References

[1] H.K. Dan, J.B. Qiu, D.C. Zhou, Q. Jiao, R.F. Wang and N.L. Thai, Materials Letters **234**, 142 (2019).

[2] Y.R. Zhu, X.J. Shen, X.E. Su, M.H. Zhou and Y.X. Zhou, Materials Letters **244**, 175 (2019).

[3] H. Algarni, M.S. Al-Assiri, M. Reben, I.V. Kityk, B. Burtan-Gwizdala, H.H. Hegazy, Ahmad Umar, E. Yousef and R. Lisiecki, Optical Materials **83**, 257 (2018).

[4] K.F. Li, H.Y. Fan, G. Zhang, G.X. Bai, S.J. Fan, J.J. Zhang and L.L. Hu, Journal of Alloys and Compounds **509**, 3070 (2011).

[5] Y.R. Zhu, X.J. Shen, X.E. Su, M.H. Zhou, Y.X. Zhou, J. Li and G.B. Yang, Journal of Non-Crystalline Solids **507**, 19 (2019).

[6] G.Y. Zhao, L.Z. Xu, S.H. Meng, C.B. Du, J.S. Hou, Y.F. Liu, Y.Y. Guo, Y.Z. Fang, M.S. Liao, J. Zou and L.L. Hu, Journal of Luminescence **206**, 164 (2019).

[7] D. Rajesh, R.J. Amjad, M.R. Dousti and A.S.S. de Camargo, Journal of Alloys and Compounds **695**, 607 (2017).

[8] H. Fares, H. Elhouichet, B. Gelloz and M. Férid, Journal of Applied Physics **117**, 193102 (2015).

[9] Z.Z. Zhou, M.H. Zhou, X.E. Su, P. Cheng and Y.X. Zhou, Optoelectronics Letters **13**, 54 (2017).

[10] Y. Wu, Y.H. Han, T.Q. Li, H.Y. Zhang, B.X. He, Y. Wang, J. Mei, Y. Chen, J.G. Feng, N. Wang, J. Zhang, C. Feng and J.J. Shen, Journal of Optoelectronics·Laser **28**, 625 (2017). (in Chinese)

[11] Y.B. Hu, J.B. Qiu, Z.G. Song, Z.W. Yang, Y. Yang, D.C. Zhou, Q. Jiao and C.S. Ma, Journal of Luminescence **145**, 512 (2014).

[12] N. Deopa, S. Kaur, A. Prasad, B. Joshi and A.S. Rao, Optics & Laser Technology **108**, 434 (2018).

[13] G.V. Rao and H.D. Shashikala, Journal of Alloys and Compounds **622**, 108 (2015).

[14] R.J. Amjad, M.R. Dousti and M.R. Sahar, Current Applied Physics **15**, 1 (2015).

[15] R.J. Amjad, M.R. Sahar, M.R. Dousti, S.K. Ghoshal and M.N.A. Jamaludin, Optics Express **21**, 14282 (2013).

[16] W.J. Zhang, J. Lin, M.Z. Cheng, S. Zhang, Y.J. Jia and J.H. Zhao, Journal of Quantative Spectroscopic and Radiative Transfer **159**, 39 (2015).

[17] Y. Zhang, C.Y. Zhang, W.B. Sun, Z.B. Zhang, E.Y.B. Pund, D.L. Zhang and W.H. Wong, Journal of Luminescence **198**, 457 (2018).

[18] F. Ahmadi, R. Hussin and S.K. Ghoshal, Journal of Luminescence **204**, 95 (2018).

[19] H. Fares, H. Elhouichet, B. Gelloz and M. Férid, Journal of Applied Physics **116**, 123504 (2014).